Global modeling of mixed-phase clouds: The albedo and lifetime effects of aerosols

T. Storelvmo,[1] C. Hoose,[2] and P. Eriksson[3]

Received 6 July 2010; revised 23 November 2010; accepted 29 November 2010; published 15 March 2011.

[1] We present a global modeling study of mixed-phase clouds and have performed sensitivity simulations to explore the ways in which aerosol particles can affect this type of cloud. This study extends previous similar studies in that it takes into account not only the so-called aerosol lifetime effects on mixed-phase clouds but also aerosol effects on their albedo. Our findings generally agree with previous studies in that an increase in ice-nucleating aerosol particles (IN) leads to a decreased cloud lifetime and therefore a warming of the Earth-atmosphere system. However, an increase in IN will also generally decrease ice crystal sizes, thereby increasing the cloud albedo, which is analogous to the well-established Twomey effect on liquid clouds. This decrease in ice crystal effective radii leads to an increase in cloud albedo and hence to a cooling that counteracts the lifetime effect of mixed-phase clouds. Taking both the albedo and lifetime effects of mixed-phase clouds into account, we find the net radiative forcing effect of an IN increase to be positive but small, which is in contrast to a much stronger warming that is found if the albedo effect is not taken into account. The latter has been the common approach in global studies of aerosol effects on mixed-phase clouds so far. Results were found to be extremely sensitive to the choice of heterogeneous freezing parameterization and the maximum fraction of black carbon particles available for ice nucleation.

Citation: Storelvmo, T., C. Hoose, and P. Eriksson (2011), Global modeling of mixed-phase clouds: The albedo and lifetime effects of aerosols, *J. Geophys. Res.*, *116*, D05207, doi:10.1029/2010JD014724.

1. Introduction

[2] The term "aerosol indirect effects" (AIEs) refers to the different ways in which aerosol particles can affect Earth's climate by modifying cloud properties. Because such aerosol perturbations of cloud properties can occur via a range of different mechanisms, and because aerosol effects can vary greatly from one cloud type to another, AIEs are often divided according to which clouds they affect. In the Intergovernmental Panel on Climate Change (IPCC) AR4 [*Denman et al.*, 2007], AIEs were divided into (1) effects on liquid clouds, (2) effects on mixed-phase clouds, and (3) effects on cirrus and/or ice clouds. These effects are sometimes also divided further into impacts on the cloud albedo and impacts on cloud lifetime. The albedo and lifetime effects of liquid clouds are also referred to as the "Twomey" effect [*Twomey*, 1977] and the "Albrecht" effect [*Albrecht*, 1989], respectively, and have both been studied extensively in laboratories and in the field using satellite data and models of different scales and resolutions. The albedo effect comes about by hygroscopic aerosols' acting as cloud condensation nuclei (CCN), thereby increasing the cloud droplet number concentration (CDNC). For a given cloud water content, such an increase in CDNC will decrease cloud droplet effective radii and increase cloud albedo. This effect is relatively well established, and the albedo effect of anthropogenic CCN was estimated in IPCC AR4 to cool the current climate, with estimates ranging from -1.9 to -0.2 W m^{-2}.

[3] The lifetime effect of liquid clouds is more controversial [*Stevens and Feingold*, 2009; *Levin and Cotton*, 2007]. While most global models predict that a CCN increase will delay precipitation and increase cloud lifetime, models with higher resolution and a more sophisticated treatment of cloud dynamics suggest that a CCN increase may in some cases lead to a reduced cloud lifetime [*Wood*, 2006]. The reason for the discrepancy between global climate models (GCMs) and models with higher resolution and more elaborate cloud schemes is suggested to be the poor representation of entrainment and mixing processes in the GCMs. While this will remain a challenge for the global modeling community in years to come, it is not the focus of the present paper.

[4] The research on aerosol effects on mixed-phase clouds is still in its infancy, and progress is currently inhibited by the lack of quantitative understanding of which aerosol particles have the ability to perturb mixed-phase clouds by forming ice crystals. While dust particles, primary biogenic particles, and black carbon (BC) particles have been suggested as

[1]Department of Geology and Geophysics, Yale University, New Haven, Connecticut, USA.
[2]Institute for Meteorology and Climate Research, Karlsruhe Institute of Technology, Karlsruhe, Germany.
[3]Department of Earth and Space Science, Chalmers University of Technology, Gothenburg, Sweden.

0148-0227/11/2010JD014724

atmospheric ice-nucleating aerosol particles (IN) candidates, their relative contributions to ice formation in mixed-phase clouds are still largely unknown. As aerosol effects on mixed-phase clouds have recently been suggested to potentially contribute to the strong warming observed at high latitudes [*Zeng et al.*, 2009; *Girard et al.*, 2004], certain questions have become more urgent, such as, What aerosol particles make good IN? and, To what extent are atmospheric IN loadings influenced by human activity?

[5] The focus of the few global modeling studies addressing aerosol effects on mixed-phase clouds has been the influence on cloud lifetime [*Lohmann and Feichter*, 2005], sometimes termed the "cloud glaciation effect" [*Lohmann and Diehl*, 2006; *Hoose et al.*, 2008; *Storelvmo et al.*, 2008a; *DeMott et al.*, 2010]. So far, global model studies have qualitatively agreed that an increase in IN concentrations increases cloud glaciation. A complete glaciation of a mixed-phase cloud is believed to be followed by precipitation due to the efficient growth of ice crystals at the expense of cloud droplets, known as the Bergeron-Findeisen (BF) process. Hence, an increase in IN is likely to decrease cloud lifetime by increasing precipitation release via the ice phase. Global studies of aerosol effects on mixed-phase clouds typically have not provided any estimates of the aerosol effect on ice crystal sizes. *Morrison and Gettelman* [2008] predicted ice crystal radii using a two-moment cloud microphysics scheme, but ice crystal formation was not linked to predicted aerosol concentrations. Ice crystal effective radii in GCMs have traditionally been prescribed to a single value or are simple functions of temperature and therefore have not been sensitive to changes in IN concentrations. However, several recent global studies have investigated perturbations in effective ice crystal radii in cirrus clouds in response to anthropogenic aerosols. For example, the studies by *Liu et al.* [2007], *Salzmann et al.* [2010], and *Gettelman et al.* [2010] predicted ice crystal effective radii on the basis of aerosol-dependent ice crystal number concentrations, but focused their study on cirrus rather than mixed-phase clouds. In cirrus clouds, homogeneous and heterogeneous freezing mechanisms may in certain cases compete for the available water vapor, with a potentially strong influence on ice crystal number concentrations and sizes. Although aerosol effects on cirrus clouds are potentially significant, they are not the focus of the present study. Here we focus on treating aerosol effects on mixed-phase clouds in a more consistent manner, as the ice crystal number concentrations calculated on the basis of available IN determine the ice crystal effective radii entering radiation calculations. *Jiang et al.* [2009] reported a negative correlation between aerosol pollution and ice crystal effective radii in convective clouds observed from space. They used high carbon monoxide (CO) values as a proxy for aerosol emissions from biomass and fossil fuel burning, and their results thus indicate that combustion particles were responsible for the difference in ice crystal sizes measured between polluted and clean cases. However, their method could not determine which microphysical mechanisms caused this difference, and further observational evidence is needed to single out the mechanisms responsible for the more numerous and smaller ice crystals in the polluted case.

[6] The remainder of this paper is structured as follows: Section 2 describes the modeling tool used in this study, in particular the treatment of mixed-phase clouds. Also presented is a description of the model simulations performed along with a description of the satellite data used for model validation. Section 3 presents and discusses the results of these simulations along with a comparison with available satellite observations. Finally, section 4 concludes the paper and outlines future research directions of interest.

2. Model Description and Experimental Setup

2.1. The Modeling Tool

[7] The modeling tool employed in this study is the aerosol-climate model Community Atmosphere Model (CAM)-Oslo, an extended version of CAM3 [*Collins et al.*, 2006]. Extensions include a sophisticated aerosol module [*Seland et al.*, 2008] describing aerosol size distributions and chemical compositions. The module treats sea salt, mineral dust, sulfate, black carbon and organic aerosols, and their size distribution are described by 16 lognormal modes and 44 size bins with process-determined mixing states. A treatment of primary biogenic aerosol particles (PBAPs) was recently implemented, but is not included here as PBAPs were found to have only minor effects on clouds and climate [*Hoose et al.*, 2010]. A subgrid-scale vertical velocity is parameterized to calculate supersaturations and the fraction of aerosol particles activated to form cloud droplets in a given gridbox. Cloud droplet activation follows the work by *Abdul-Razzak and Ghan* [2000] with modifications by *Hoose et al.* [2009]. As the focus of this study is mixed-phase clouds (MPCs), we describe modifications to the standard CAM3 cloud microphysics below from a MPC point of view.

2.2. The Mixed-Phase Cloud Scheme

[8] The microphysical evolution of mixed-phase clouds is governed by four continuity equations predicting the cloud liquid water content and ice water content (IWC) as well as the cloud droplet and ice crystal number concentrations [*Storelvmo et al.*, 2006; *Storelvmo et al.*, 2008a]. Parameterization schemes that carry both cloud condensate and cloud particle concentrations (i.e., the third moment and zeroth moment of the cloud particle size distribution, respectively) as prognostic variables are often referred to as double-moment microphysics schemes. In contrast to in-cloud water and ice, precipitating water and ice are diagnosed quantities in this model. All precipitaion formed in-cloud over a time step is assumed to either reach the surface or sublimate and/or evaporate in subcloud gridboxes over the course of the same time step.

[9] The advantage of in-cloud double-moment microphysics schemes compared with schemes that predict cloud condensate only is that they allow for prediction of the time evolution of cloud particle sizes for a given assumption of the shape of the size distribution. The cloud particle sizes in turn determine the amount of precipitation formed as well as cloud optical properties. The following continuity equation for ice crystal number concentration (ICNC) is thus of particular relevance for this paper:

$$\frac{dN_i}{dt} = A_{N_i} + frz_{\mathrm{imm}} + frz_{\mathrm{cnt}} + frz_{\mathrm{dep}} + frz_{\mathrm{hom}} + mult - aut - saci - mlt - slfc - subl \quad (1)$$

[10] Its source terms are heterogeneous ice crystal formation (immersion and/or condensation (frz_{imm}), contact

Table 1. Short Description of the Six Simulations Carried Out in This Study[a]

Simulation	Description
BC	Heterogeneous freezing follows *Diehl et al.* [2006], and mineral dust and accumulation mode BC act as IN
*BC*10	Same as for *BC*, but only 10% of accumulation mode BC may act as IN
*BC*01	Same as for BC, but only 1% of accumulation mode BC may act as IN
*CNT*01	Heterogeneous freezing based on *Hoose et al.* [2010], with fraction of BC particles available as IN limited to 1%
*CNT*001	Same as for *CNT*01, but fraction of BC particles available as IN is limited to 0.1%
CFDC	Heterogeneous freezing based on *DeMott et al.* [2010]

[a]BC, black carbon; IN, ice-nucleating aerosol particles.

freezing (frz_{cnt}), deposition nucleation (frz_{dep}), homogeneous freezing (frz_{hom}), and the ice multiplication process known as the Hallett-Mossop process (*mult*) [*Hallett and Mossop*, 1974]. Ice crystals are lost as a result of self-collection (*slfc*), precipitation formation (*aut*), collection by snow falling from above (*saci*), melting (*mlt*), and sublimation (*subl*). Furthermore, ice crystals are subject to sedimentation; horizontal advection; and convective, turbulent, and diffusive transport (A_{Ni}). For the details of the microphysical terms in equation (1), see *Storelvmo et al.* [2008a] and *Rasch and Kristjánsson* [1998]. Homogeneous and heterogeneous freezing at cirrus levels are not explicitly accounted for, and ice crystal formation below −38°C follows the simplified approach of *Lohmann* [2002]. For the temperature range from −38°C to 0°C, the heterogeneous freezing processes follow the approach of *Diehl et al.* [2006], *Hoose et al.* [2010], or *DeMott et al.* [2010]. The three parameterization schemes are based on, respectively, (1) laboratory measurements only, accounting for immersion and/or condensation and contact freezing; (2) a combination of classical nucleation theory and laboratory measurements, accounting for contact, immersion and/or condensation, and deposition freezing; and (3) observations from field studies of immersion and/or condensation and deposition freezing. A new subgrid treatment of the process of cloud glaciation (i.e., the BF process) was introduced by *Storelvmo et al.* [2008b] and *Storelvmo et al.* [2010] on the basis of theoretical and observational work by *Korolev* [2007], *Korolev and Mazin* [2003], and *Korolev and Isaac* [2006]. On the basis of a subgrid distribution of vertical velocity, the corresponding distribution of supersaturation with respect to water and ice is calculated accounting for water vapor depletion by condensational and/or depositional growth of cloud droplets and ice crystals. On the basis of the description above, each gridbox is divided into regions characterized by (1) crystal and droplet growth, (2) the BF process, and (3) droplet evaporation and crystal sublimation. The Hallett-Mossop process is calculated following the formulation described by *Levkov et al.* [1992].

[11] From the ice crystal number concentration and IWC of the mixed-phase clouds, a mean volume radius (r_v) for the ice crystals can be calculated. However, since cloud optical properties are parameterized as a function of the ice crystal effective radius ($r_{e,i}$; for a definition, see, e.g., *Wyser* [1998]), we convert from r_v to $r_{e,i}$ following *Liu et al.* [2007]. The conversion is based on the assumption that the relationship $r_v^3 = kr_{e,i}^3$ holds true and that the ice crystal size distribution can be described by a power law spectrum where the power exponent is dependent on the IWC and temperature (T) of the cloud. Using this assumption, it follows that k is a function of IWC and T. In the model, ice cloud optical properties for a given model layer are determined by $r_{e,i}$ (μm) and the vertically integrated IWC, often referred to as the ice water path (IWP; g m^{-2}). The shortwave ice cloud optical thickness follows the parameterization described by *Ebert and Curry* [1992]:

$$\tau_{cld,i}^{i} = IWP\left(a^i + \frac{b^i}{r_{e,i}}\right), \tag{2}$$

where the superscript i denotes the spectral interval and the constants a and b are wavelength dependent and given by *Ebert and Curry* [1992]. The longwave emissivity is given by the followng approximation:

$$\varepsilon_{cld,i} = 1 - \exp(-1.66 k_{\mathrm{abs}} IWP), \tag{3}$$

where k_{abs} is the absorption coefficient for ice clouds and is based on a broadband fit to the emissivity given by *Ebert and Curry* [1992]:

$$k_{\mathrm{abs}} = 0.005 + \frac{1}{r_{e,i}} \tag{4}$$

2.3. Satellite Observations

[12] In section 3.1, model output is compared to satellite data, including CloudSat retrievals. The CloudSat Cloud Profiling Radar is a 94 GHz active instrument measuring cloud backscattering as a function of altitude [*Stephens et al.*, 2002]. The satellite is in a Sun-synchronous orbit with a 13:31 h (local time) ascending node. The footprint size is about 2 km^2, and the vertical resolution is approximately 500 m. These observations give detailed information about cloud structures, but various microphysical variables are also retrieved that are constrained in varying degrees by the observed backscattering. The retrievals were taken from the Level Radar-Only Cloud Water Content, or 2B-CWC-RO (R04), product.

[13] The first considered CloudSat retrieval quantity is the vertical integral of IWC, i.e., the IWP. Systematic errors for IWC have been estimated to be less than 40%, and the CloudSat radar does not allow for a discrimination between liquid and ice particles [*Austin et al.*, 2009]. The IWP retrieval can thus have significant biases, but we are not aware of any detailed error estimate. Other factors to consider for a model comparison is the diurnal sampling [*Eriksson et al.*, 2010] and the fact that the radar does not discriminate between nonprecipitating and precipitating particles [*Waliser et al.*, 2009].

[14] IWP has also been derived from the International Satellite Cloud Climatology Project (ISCCP) [*Rossow and Schiffer*, 1999]. The IWP is produced here by summing up the partial IWP for ISCCP's three cloud types. The method follows the work by *Storelvmo et al.* [2008a], with minor corrections affecting only high-latitude values. The ISCCP data set is based on visible and infrared data. Radiation at such wavelengths interacts primarily with smaller ice particles and cannot detect, e.g., multilayer clouds. It is assumed

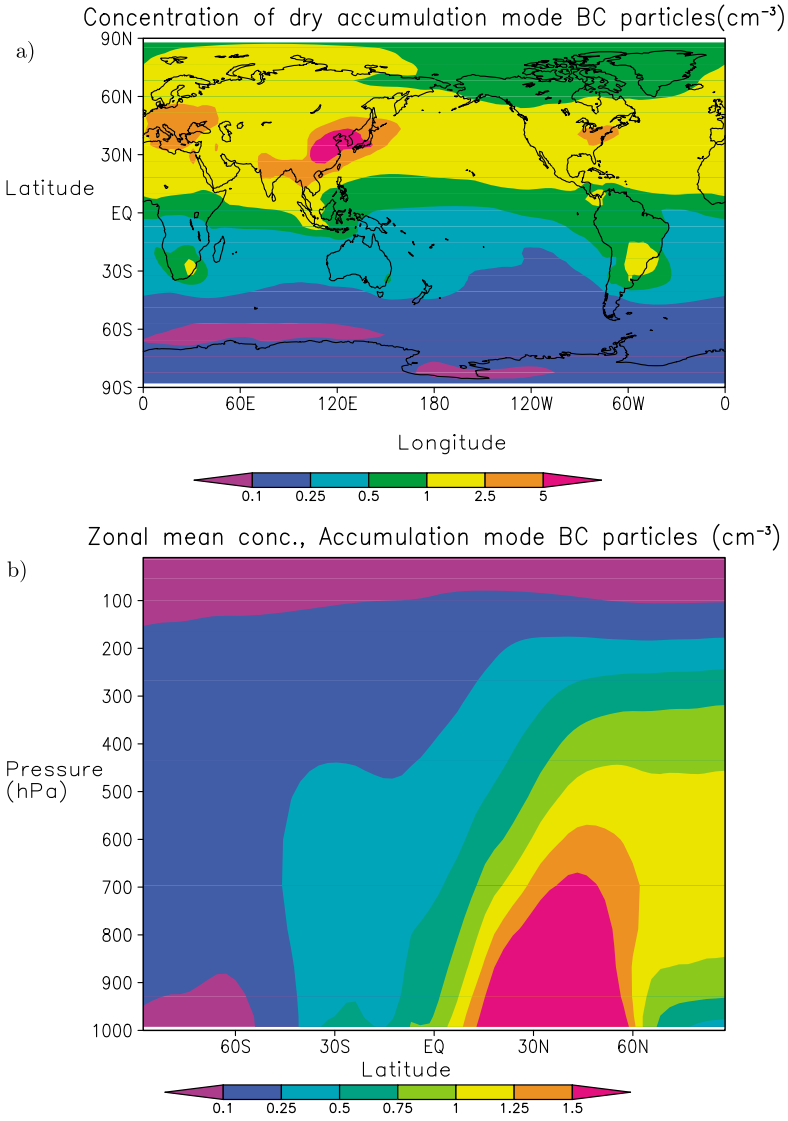

Figure 1. Annual average concentrations of dry, i.e., externally mixed, black carbon (BC) accumulation mode particles: (a) 930 hPa and (b) zonal mean.

here that the ISCCP IWP represents the nonprecipitating ice mass rather than the total ice mass. More detailed discussion and comparison of IWP data sets, including CloudSat and ISSCP, are found in the publication by *Eliasson et al.* [2010].

[15] A second considered CloudSat retrieval quantity is effective radius. A single-wavelength radar lacking Doppler capability such as CloudSat gives no direct constraint on particle sizes, and IWC can be seen as the main microphysical retrieval quantity. From this perspective, the effective radius reported largely follows the retrieved IWC. In short, a higher measured backscattering will result not only in higher IWC but also smaller effective radius. The relationship between IWC and particle size constitutes important a priori information that is taken from in situ observation campaigns [*Austin et al.*, 2009].

2.4. Experimental Setup

[16] We have carried out six 5-year simulation experiments, each with a spin-up of 4 months. The horizontal resolution for all simulations is T42 (2.8125° × 2.8125°) with 26 vertical levels. Emissions of aerosols and aerosol precursor gases were taken from the work by *Dentener et al.* [2006]. Each experiment was carried out four times: with and without the albedo effect included and with and without anthropogenic BC (referred to as present-day (PD) and preindustrial (PI) versions of the same simulation). In simulations that do not allow aerosol effects on the cloud albedo, ice crystal effective radii are calculated as a function of temperature only, following the parameterization by *Kristjánsson et al.* [2000]. The simulations are summarized in Table 1. In the simulations, dust particles and accumulation mode BC particles were available for ice nucleation. The simulations were carried out twice: once with all aerosol emissions corresponding to PD conditions and the other with PI BC emissions. All aerosol emissions other than BC were the same in both simulations. This experimental setup allows us to isolate and investigate the effect of increased IN concentrations on mixed-phase clouds. In simulations *BC*10

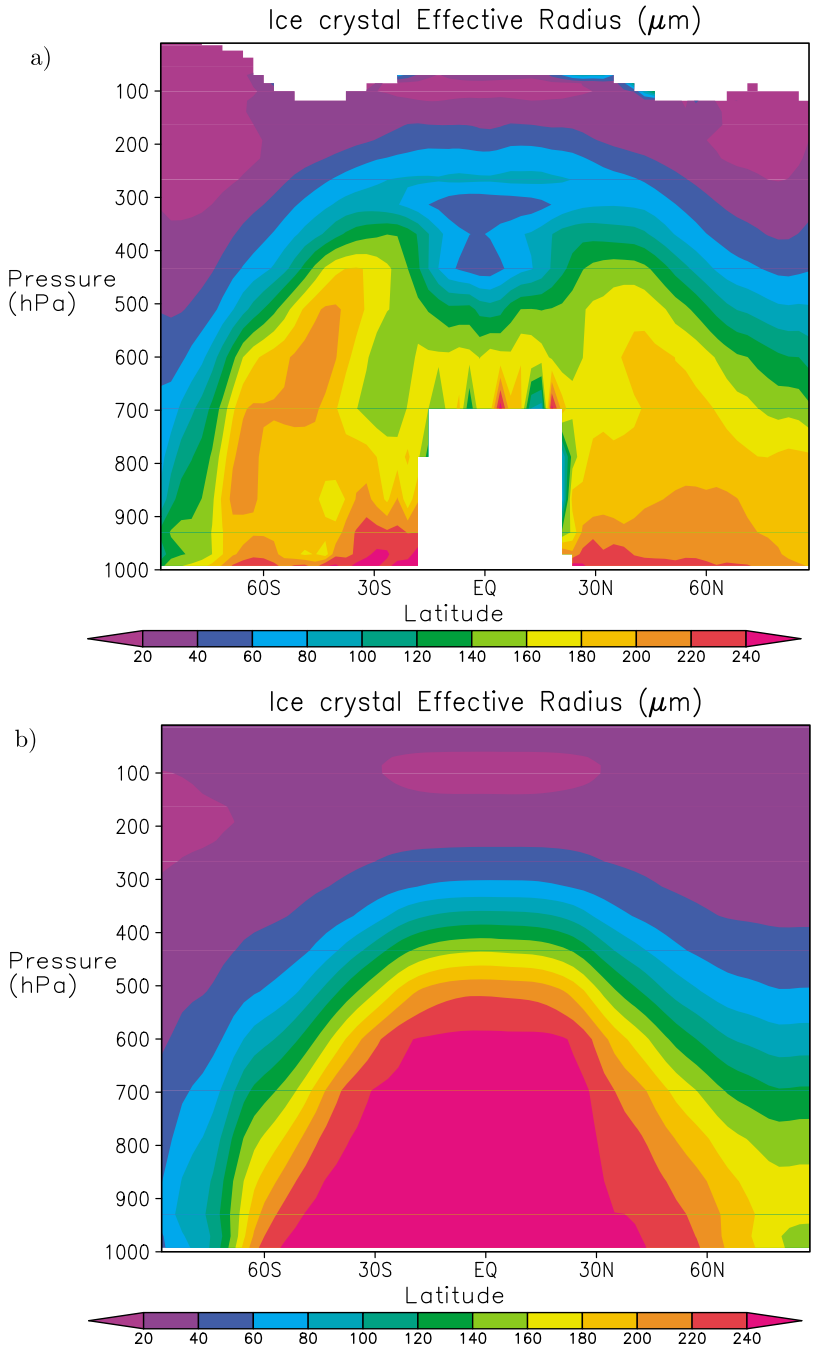

Figure 2. Annual and zonal mean effective radii (a) as calculated from prognostic ice crystal number concentrations and (b) as diagnosed using the empirical relationship from *Kristjánsson et al.* [2000].

and simulations *BC*01, the accumulation mode BC particles available for ice nucleation were limited to 10% and 1 %, respectively. In simulations *CNT*01 and *CNT*001, the alternative parameterization of heterogeneous freezing by *Hoose et al.* [2010] was applied with an upper limit for the fraction of BC particles acting as IN of 1% and 0.1 %, respectively. In simulation CFDC, the new parameterization of heterogeneous freezing by *DeMott et al.* [2010] was applied. This range of simulations varying the heterogeneous freezing scheme and the fraction of aerosol active as IN is motivated by recent studies suggesting that the standard parameterization by *Diehl et al.* [2006] may significantly overestimate ice nucleation rates and ice crystal number (e.g., *Eidhammer et al.* [2010]).

[17] Figure 1a shows the annual average global distribution of externally mixed accumulation mode BC particles from the PD simulation (shown for the 930 hPa level). A large fraction of the BC particles residing in the accumulation mode stem from fossil fuel emissions of agglomerated BC, consistent with a somewhat aged but not entirely collapsed agglomerate structure [*Seland et al.*, 2008]. The relevance of such particles is supported by, e.g., *Bond et al.* [2006]. Thus high concentrations are associated with regions of high fossil fuel emissions such as East Asia, Europe, and

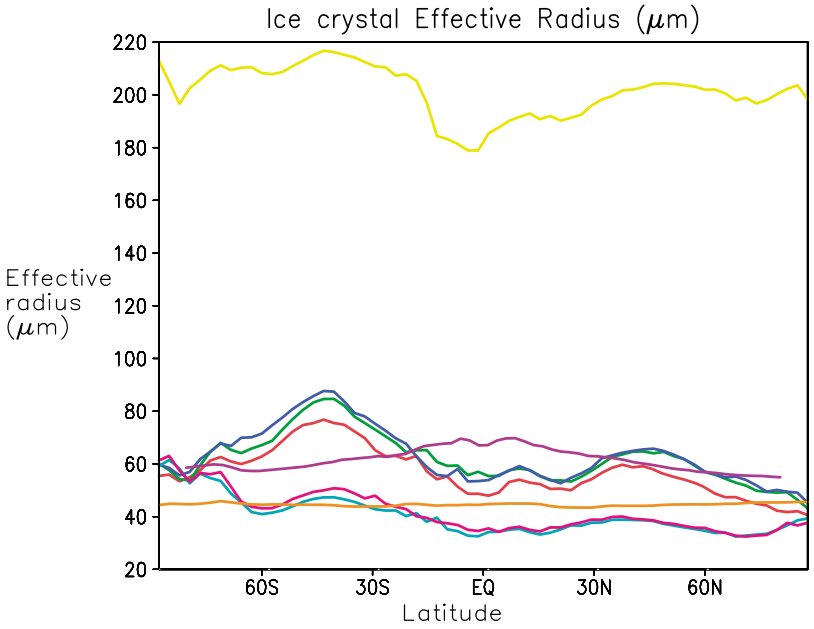

Figure 3. Annual and zonal mean effective radii at 240 K from present-day simulations *BC* (red), *BC*10 (green), *BC*01 (blue), *CNT*01 (pink), *CNT*001 (turqoise), *CFDC* (yellow), the empirical relationship from *Kristjánsson et al.* [2000] (orange), and CloudSat (purple).

the eastern United States. Figure 1b shows the corresponding zonal mean concentrations as a function of pressure, illustrating that high concentrations are confined to the Northern Hemisphere at all levels, and that accumulation mode particles are efficiently transported northward with height, yielding relatively high concentrations in Arctic regions. Although BC particles are largely hydrophobic, they may become hydrophilic as they age chemically and are coated by soluble species. Nevertheless, their effects on liquid clouds are essentially negligible in the model (not shown), and cloud droplet number concentrations are therefore very similar in PD and PI simulations. Direct radiative effects and semidirect effects of aerosols do not differ among the simulations (by using the same prescribed aerosol fields for aerosol interaction with radiation in all simulations), nor do aerosol effects on cirrus clouds (i.e., clouds with temperatures below −38°C). Ice crystal concentrations for these clouds are calculated as described by *Lohmann* [2002].

[18] Laboratory results indicate that compared with natural IN such as mineral dust and biological particles, soot is the least efficient IN (see, e.g., *Kärcher et al.* [2007] and *Möhler et al.* [2005]). However, in situ observations indicate an enrichment of soot in atmospheric ice particle residuals in lower tropospheric mixed-phase clouds [*Cozic et al.*, 2008; *Targino et al.* [2009]. There are suggestions that soot may act as a contact IN at temperatures between −22°C and −28°C [*Diehl and Mitra*, 1998; *Fornea et al.*, 2009]. Acetylene burner soot has been observed to initiate immersion freezing at similar temperatures [*DeMott*, 1990]. However, some of these laboratory studies suffer from particle or droplet sizes that are not necessarily representative for the atmosphere, and more experiments with conditions that are relevant for the atmosphere are needed. Although IN perturbations are realized in this study by changing BC concentrations, we would expect the results to be qualitatively similar if IN concentrations increased as a result of, e.g., desertification and increased mineral dust concentrations. However, the geographical emission distributions, and therefore the regional cloud responses, would inevitably be very different.

3. Results and Discussion

3.1. Validation of Modeled Ice Water Path and Ice Crystal Effective Radius

[19] Crucial parameters for determining the radiative effects of mixed-phase cloud glaciation are the IWP and the effective radius of the ice crystals ($r_{e,i}$) (see equations (2)–(4)). For comparison with observations, we have chosen the PD version of experiment BC01 as our control simulation. In Figures 2a and 2b, the simulated zonal and annual mean ice crystal effective radius is compared to $r_{e,i}$ predicted by an empirical relationship between ice crystal effective radii and temperature reported by *Kristjánsson et al.* [2000]. The empirical relationship stems from field observations by *Ryan* [1996] and *McFarquhar and Heymsfield* [2002]. Overall, the simulated and empirical effective radii both decrease with height and span the same size ranges. As expected, the predicted ice crystal radii show more variability, as they are sensitive to the predicted ice crystal number concentrations and therefore the IN availability. Figure 3 shows the zonal mean effective radii as predicted in all six simulations and by the empirical relationship described by *Kristjánsson et al.* [2000] at a temperature of 240 K compared with the equivalent field obtained from CloudSat observations. We chose this temperature for comparison because CloudSat retrievals cannot distinguish between liquid and ice and therefore rely on temperature as a proxy for the presence of ice. Choosing a temperature low

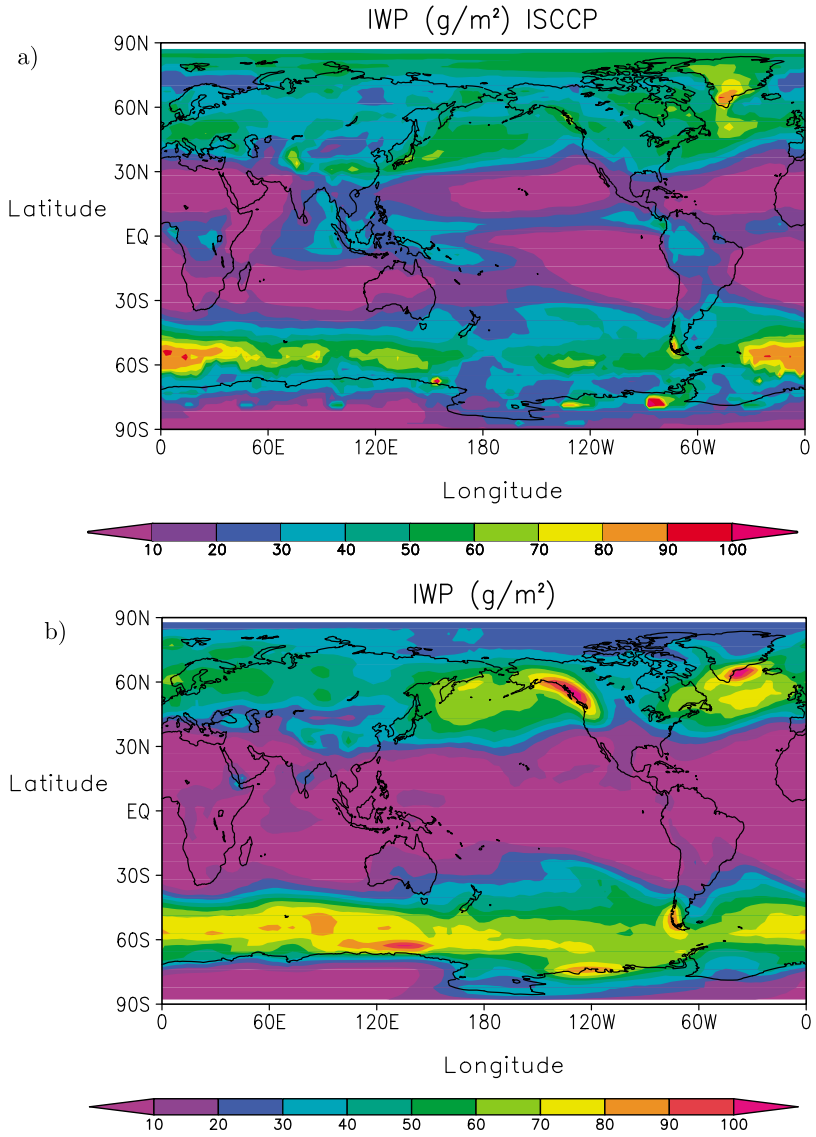

Figure 4. Vertically integrated ice and snow from (a) the International Satellite Cloud Climatology Project (ISCCP) data set and (b) simulation *BC*01.

enough for most clouds to consist of ice while comparing ice clouds that most likely formed heterogeneously, the comparison is relevant for mixed-phase clouds and most likely not affected by CloudSat misinterpreting cloud droplets as ice crystals. Effective radii from the model are sampled from the temperature interval 235 K to 245 K. The simulated size ranges and the annual and global average values agree reasonably well with observations, with the exception of simulation *CFDC*. The parameterized ice nuclei in this simulation are a function of temperature and the concentration of insoluble aerosol particles larger than 0.5 μm. The concentrations of such large particles decrease rapidly with height in the model, and at the level of the coldest MPCs the concentrations are very low, which translates into low ice crystal number concentrations (on the order of 1 l^{-1}) and large effective radii. However, the comparison with observations is not perfect for other simulations either, and Figure 3 reveals that most simulations show an interhemispheric contrast that is not evident in the satellite data. There are several possible explanations for this disagreement with the observations. First, the two aerosol species available for ice nucleation in the simulations, mineral dust and BC, both have much higher concentrations in the Northern Hemisphere. Missing dust or BC sources in the Southern Hemisphere or too weak transport across the equator could explain the exaggerated interhemispheric contrast. Second, in the case of asymmetric IN concentrations across the equator, ice multiplication processes would contribute to reducing the interhemispheric contrast in ice crystal number. Among the ice multiplication mechanisms proposed in the literature (e.g., *Pruppacher and Klett* [1997]), only the so-called Hallett-Mossop process [*Hallett and Mossop*, 1974] is currently included in the model.

[20] A third reason for disagreements between simulated and observed ice crystal radii could be that the amount of cloud ice in the model is poorly predicted. However, Figure 4 suggests that this is not the case, showing simulated IWP compared with that observed by satellite in the ISCCP

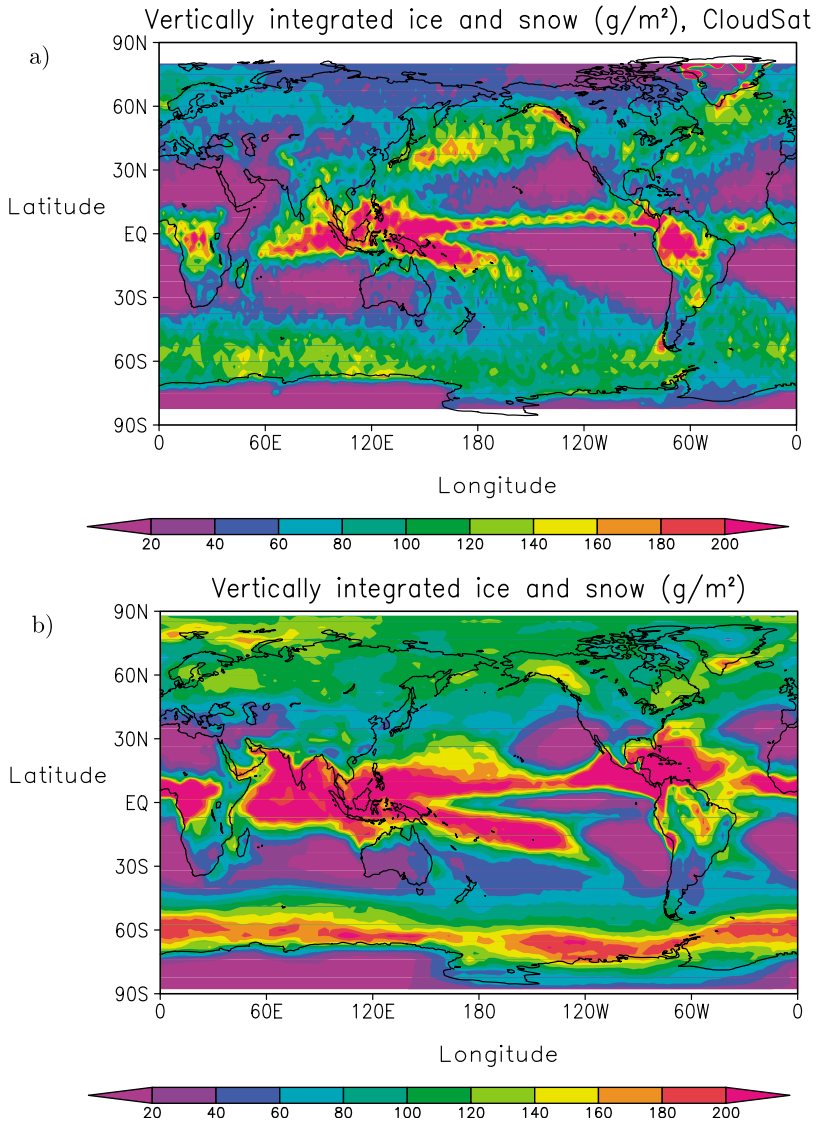

Figure 5. Ice water path from (a) CloudSat and (b) simulation *BC*01.

data set. Although an underestimation of cloud ice is evident in the tropics and a slight overestimation can be seen for midlatitude storm tracks, simulated and observed values compare fairly well. Figure 5 shows vertically integrated ice and snow from CloudSat compared to simulation *BC*01. The Cloudsat radar cannot distinguish in-cloud ice crystals from falling snow crystals, so in this case all falling snow must be included for a given model column for a fair comparison. Also in this case, the simulated and observed values compare fairly well, although the model simulation seems to slightly overestimate atmospheric ice and snow. This is also true for the tropics, which suggests that in tropical clouds precipitation forms too rapidly in the model after conversion from liquid to ice to have occurred.

3.2. The Cloud Lifetime Effect

[21] As seen in Table 2, the additional IN here represented by anthropogenic BC in the PD simulation lead to a decrease in cloud lifetime and therefore a reduction in both the liquid water path (LWP) and IWP. The reduced cloud lifetime in the presence of high IN concentration comes about as a result of the BF process, in which ice crystals coexisting with cloud droplets will inevitably grow at the expense of the liquid droplets. The increase (PD – PI values) in the fraction of the clouds where the BF process takes place is presented in Figure 6 as a function of pressure (i.e., height) and shows that in simulation *BC* there is a pronounced increase in the cloud fraction dominated by the BF process, while simulations *BC*10, *BC*01, and *CNT*01 show more moderate increases. Simulations *CNT*001 and *CFDC* showed no significant changes and are not included in Figure 6.

[22] As the ice crystal concentrations are generally orders of magnitude smaller than the typical cloud droplet number concentrations, the BF process will redistribute the cloud water onto fewer cloud particles, which can either grow large enough to sediment out from the cloud efficiently and/or increase collision and coalescence processes because of their higher falling speeds. In both cases, the result is efficient precipitation formation, which acts to deplete cloud

Table 2. Annual Global Mean Changes in Cloud Microphysical and Radiative Properties Between Simulations with Present-Day Black Carbon and Simulations With Preindustrial Black Carbon Concentrations, Accounting Only for the Lifetime Effect on Mixed-Phase Clouds[a]

Simulation	*BC*	*BC*10	*BC*01	*CNT*01	*CNT*001
Cloud cover (%)	68.0 ± 0.05	68.3	68.3	67.6	67.8
Δ Cloud cover (%)	−0.20 ± 0.04	0.03	0.40	−0.02	0.01
LWP (g/m^2)	76.2 ± 0.16	78.3	76.3	66.6	67.5
Δ LWP (g/m^2)	−2.68 ± 0.17	−1.20	−0.42	−1.33	−0.23
IWP (g/m^2)	24.6 ± 0.03	25.6	25.8	21.1	22.2
Δ IWP (g/m^2)	−1.1 ± 0.04	−0.37	−0.21	−0.25	−0.10
SWCF, TOA (W/m^2)	−51.0 ± 0.06	−52.0	−51.1	−48.0	−48.3
Δ SWCF, TOA (W/m^2)	1.18 ±0.07	0.54	0.10	0.31	0.06
LWCF, TOA (W/m^2)	25.8 ± 0.03	26.1	25.8	22.1	22.1
Δ LWCF, TOA (W/m^2)	−0.47 ± 0.04	−0.18	0.03	−0.05	0.06
NCF, TOA (W/m^2)	−25.2 ± 0.06	−25.9	−25.3	−25.9	−26.2
Δ NCF, TOA (W/m^2)	0.71 ± 0.06	0.36	0.13	0.26	0.12

[a]Standard errors are given for simulation *BC*, are comparable to the other simulations, and are calculated on the basis of annual global means for each of the 10 simulation years. LWP, liquid water path; IWP, ice water path; SWCF, shortwave cloud forcing; TOA, top of the atmosphere; NCF, net cloud forcing.

water and results in a reduced cloud lifetime. Consequently, the lifetime effect is reversed compared with liquid clouds. The new subgrid treatment of the BF process recently developed for CAM-Oslo enables more realistic simulation of this process, which is crucial to mixed-phase cloud evolution. The reductions in IWP and LWP (hereafter referred to as total water path (TWP)) reduce cloud optical thickness and allow more solar radiation to reach the surface (as shown in equation (1)), where a large surface-albedo-dependent fraction is efficiently absorbed. Hence, the shortwave radiative response to a reduction in TWP is a heating of the Earth-atmosphere system, amounting to a reduction in shortwave cloud forcing (SWCF, defined as the reduction in downwelling shortwave radiation between clear and cloudy skies at the top of the atmosphere (TOA)) of 1.18 W m^{-1} in simulation *BC*. However, in contrast to the lifetime effect on liquid clouds, the lifetime effect on MPCs also strongly influences the amount of longwave radiation re-emitted into space. Because liquid clouds are generally optically thick and located close to the surface, they are essentially black bodies with respect to terrestrial radiation and emit radiation with an effective black body temperature very similar to the surface. Mixed-phase clouds, on the other hand, are different in both of these aspects: they are typically optically thinner and located in the middle troposphere at midlatitudes. Consequently, the increased glaciation may reduce cloud emissivity (see equation (2)) and turn MPCs into gray bodies in the longwave part of the spectrum (after glaciation), meaning that more radiation emitted from the surface is transmitted through the clouds and escapes to space rather than being absorbed and re-emitted both downward and upward with a lower intensity determined by the cloud temperature. In *BC*, this results in a longwave cloud forcing (LWCF, defined as the difference in downwelling longwave radiation at the TOA between clear and cloudy skies) of −0.47 and −0.18 W m^{-2} in simulations *BC* and *BC*10 (i.e., a cooling) and no significant effect in simulation *BC*01. The net radiative effect of the reduced lifetime of mixed-phase clouds is dominated by the shortwave effect and amounts to a warming of the Earth-atmosphere system of 0.71, 0.36, and 0.13 W m^{-2} in simulations *BC*, *BC*10, and *BC*01, respectively. The forcing in simulation *BC* is probably unrealistically large and can likely be viewed as an upper bound for the effect of anthropogenic BC on mixed-phase clouds. Hence, the net radiative forcing strongly depends on the difference in

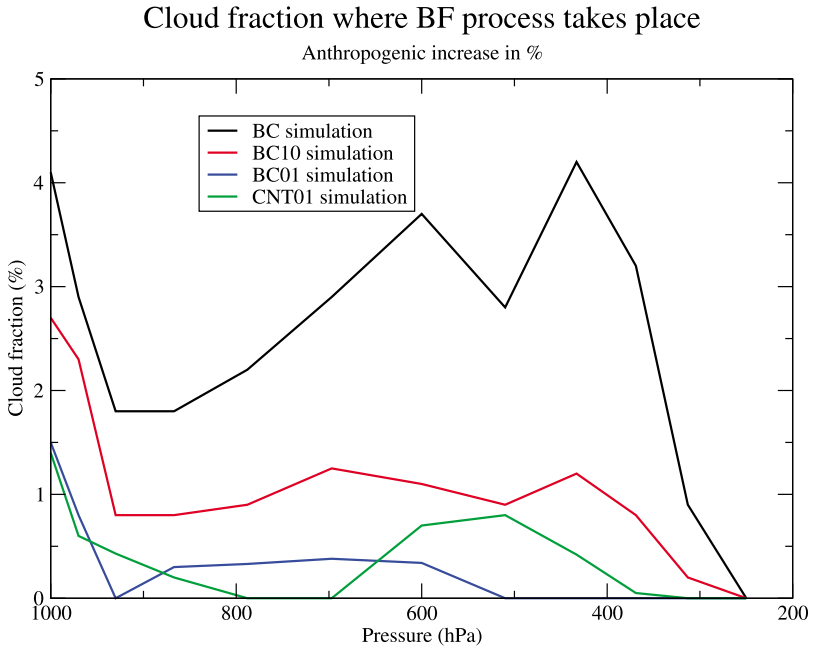

Figure 6. Change in cloud fraction where the Bergeron-Findeisen (BF) process takes place for simulations *BC* (black), *BC*10 (red), *BC*01 (blue), and *CNT* (green), calculated by subtracting the preindustrial from the present-day values.

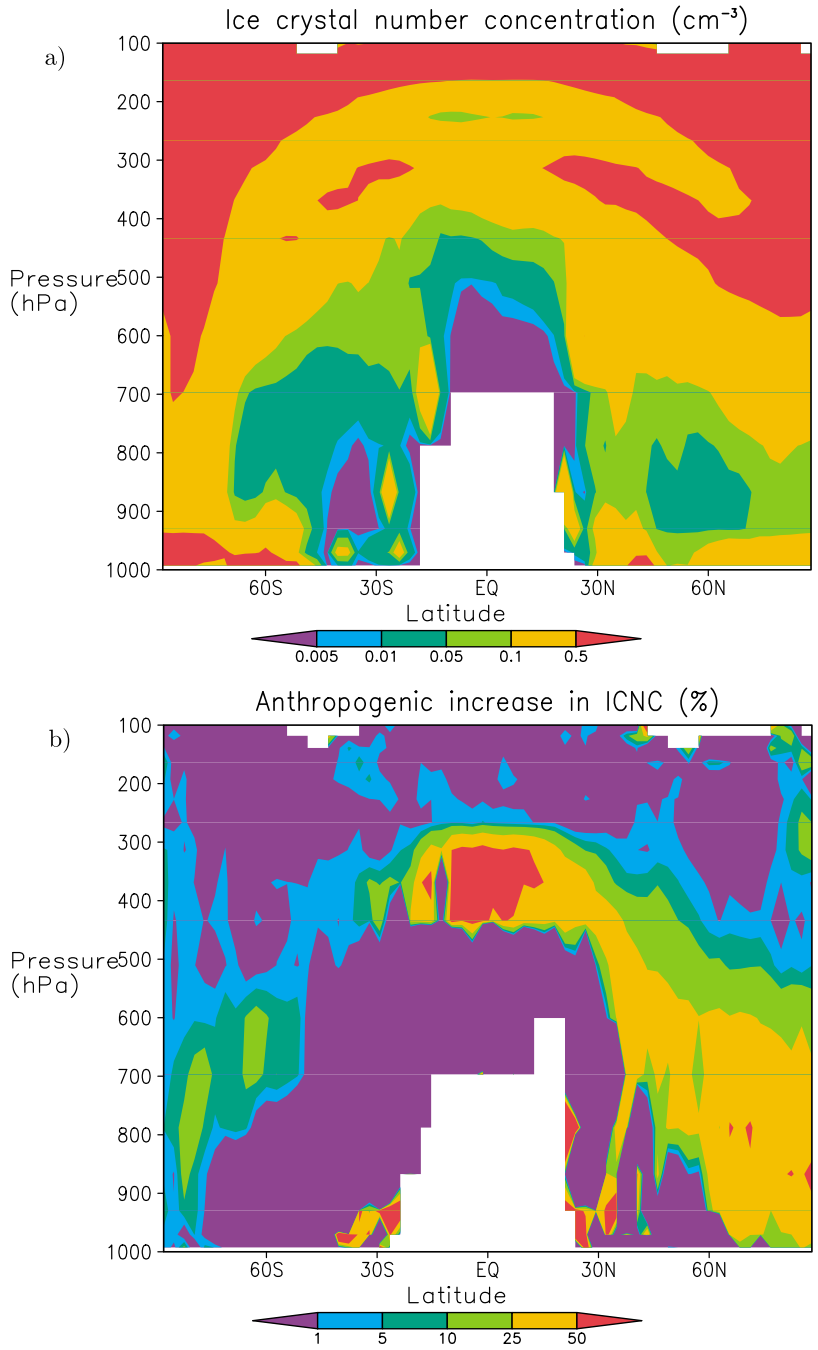

Figure 7. (a) Zonal mean ice crystal number concentrations as simulated with present-day BC emissions. (b) The percentage increase in ice crystal number concentration (ICNC) with respect to the simulation with preindustrial BC emissions. From simulation *BC*01.

IN concentrations between the PD and PI simulations, as evidenced by the more moderate positive forcings in simulations *BC*10 and *BC*01. This reduction is explained by the much more modest reduction in TWP in these simulations when PD BC is introduced.

3.3. The Cloud Albedo Effect

[23] As explained in section 1, we consider the simulations, including radiative effects of changes in $r_{e,i}$, to be an important step toward a more consistent treatment of MPC microphysical and optical properties because the predicted ice crystal number concentrations are allowed to influence not only cloud glaciation and precipitation release but also the ice crystal effective radii entering the radiation transfer calculations for MPCs. The outcome of simulations including the cloud albedo effect (in addition to the lifetime effect) of mixed-phase clouds are summarized in Table 3. As evident from Figures 7a and 7b, ice crystal number concentrations are higher in simulations including anthropogenic BC, in particular at Northern Hemisphere midlatitudes and high latitudes. ICNCs are shown for the *BC*01 simulation. The higher ICNCs combined with the lower

Table 3. Annual Global Mean Changes in Cloud Microphysical and Radiative Properties Between Simulations With Present-Day BC and Simulations With Preindustrial BC Concentrations, Accounting for Both Albedo and Lifetime Effects on Mixed-Phase Clouds[a]

Simulation	*BC*	*BC*10	*BC*01	*CNT*01	*CNT*001	*CFDC*
Cloud cover (%)	68.0 ± 0.05	67.9	68.1	67.5	67.7	67.9
Δ Cloud cover (−0.20%)	±0.04	−0.18	0.05	0.05	−0.03	0.04
LWP (g/m^2)	76.2 ± 0.16	77.5	78.5	66.2	66.8	100.2
Δ LWP (g/m^2)	−2.68 ± 0.17	−1.66	−0.55	−1.48	−0.55	0.27
IWP (g/m^2)	24.6 ± 0.03	25.5	25.8	21.3	21.5	21.0
Δ IWP (g/m^2)	−1.1 ± 0.04	−0.31	0.03	−0.27	0.03	0.12
SWCF, TOA (W/m^2)	−51.0 ± 0.06	−52.0	−52.4	−49.7	−49.7	−55.0
Δ SWCF, TOA (W/m^2)	0.67 ± 0.07	0.34	0.10	0.29	0.20	−0.39
LWCF, TOA (W/m^2)	25.8 ± 0.03	26.0	26.2	22.0	22.1	27.4
Δ LWCF, TOA (W/m^2)	−0.44 ± 0.04	−0.18	−0.03	−0.16	−0.05	0.07
NCF, TOA (W/m^2)	−25.2 ± 0.06	−26.0	−26.2	−27.7	−27.6	−27.6
Δ NCF, TOA (W/m^2)	0.23 ± 0.06	0.16	0.07	0.13	0.15	−0.32
$r_{e,i}$, cloud top (μm)	85.7 ± 0.1	93.8	97.0	62.1	62.1	131.7
Δ $r_{e,i}$, cloud top (μm)	−13 ± 0.1	−5.4	−1.7	−2.6	−1.0	−0.4

[a]Standard errors are given for simulation *BC*, are comparable to the other simulations, and are calculated on the basis of annual global means for each of the 10 simulation years.

IWC in the PD case lead to generally smaller ice crystal effective radii, as evident in Table 3 for effective radii sampled from the model as they would be observed by satellites (from the topmost ice cloud with optical thickness >0.3 and correcting for contributions from lower ice clouds in the case of partial cloud cover). The reduction in ice crystal effective radii (i.e., the albedo effect) in turn increases cloud albedo (see equation (1)), thereby counteracting the lifetime effect on the shortwave radiation. While the albedo and lifetime effects of liquid clouds both act to increase cloud albedo, the albedo and lifetime effects on the albedo of MPCs compete. In all simulations, including the albedo effect significantly reduces the net radiative effect of the IN increase. Again, mixed-phase clouds differ from liquid clouds in that their influence on longwave radiation is sensitive to changes in cloud particle radius. While the longwave cloud emissivity of liquid clouds is parameterized independently of the cloud droplet effective radius, $r_{e,i}$ influences the emissivity of glaciated clouds through equations (2) and (3). Hence, the reductions in $r_{e,i}$ in the PD versus the PI simulation render the clouds less transparent in the longwave part of the spectrum, thereby partly counteracting the longwave lifetime effect. These effects combined lead to a smaller difference in the net cloud forcing (NCF = SWCF + LWCF) between the PI and PD simulations when the albedo effect is taken into account. In simulations *BC*, *BC*10, and *BC*01, the change in NCF is reduced to 0.23, and 0.16, and 0.07 W m^{-2}, respectively, compared with 0.71, and 0.36, and 0.13 W m^{-2}, respectively, without the albedo effect.

3.4. Sensitivity to Heterogeneous Freezing Parameterization

[24] As we consider the most uncertain aspect of the model simulations to be the treatment of heterogeneous freezing, we have carried out sensitivity simulations where the standard heterogeneous freezing scheme was replaced by (1) a recently developed scheme based on classical nucleation theory [*Hoose et al.*, 2010] (simulations *CNT*01 and *CNT*001) and (2) a recently developed empirical scheme based on in situ measurements with a continuous flow diffusion chamber [*DeMott et al.*, 2010] (simulation *CFDC*, which was carried out only with the albedo effect included). The outcomes of these sensitivity simulations are shown in Tables 2 and 3 (simulation *CFDC* was only carried with both the lifetime and albedo effects included and therefore appears only in Table 3). While simulations *CNT*01 and *CNT*001 qualitatively produce results similar to those with the standard heterogeneous freezing scheme, the *CFDC* simulation shows the opposite effect. In this experiment, the dependence of ice nucleation on the concentration of large particles (which are typically of natural origin) leads to less ice formation in the PD simulation. We suggest that this is due to a shorter lifetime of large (and often natural) particles in the atmosphere because they age chemically at a faster rate in the polluted PD simulation than in the cleaner preindustrial counterpart. Consequently, cloud lifetimes are increased, and the net radiative effect is negative.

4. Conclusion and Future Work

[25] We have demonstrated that in global simulations of aerosol effects on mixed-phase clouds, the cloud albedo effect resulting from an IN increase can be of comparable magnitude to the cloud lifetime effect of the IN change. In terms of radiative forcing, the albedo effect counteracts a major part of the lifetime or glaciation effect, causing the net radiative forcing to be positive but weak in simulations with our standard heterogeneous freezing parameterization. This is in contrast to the relatively strong warming found here and in previous studies when only the lifetime effect was taken into account. These results strongly suggest that aerosol effects on mixed-phase clouds cannot be simulated realistically unless the predicted ice crystal number concentrations are allowed to interactively influence the cloud albedo in the models by modifying the ice crystal effective radii entering radiation calculations. Furthermore, we have carried out sensitivity simulations varying the fraction of BC particles available as IN and the heterogeneous freezing scheme applied to determine the number concentration of nucleated ice crystals. We find the magnitude and even the sign of the radiative forcing in response to a BC perturbation to be sensitive to the choices for the above. Parameterizations seem to differ depending on whether they are based on theoretical considerations, laboratory studies, or field observations. Simulations with the latter stand out in this study by yielding a negative radiative forcing in response to increased BC concentrations, in contrast to the consistently positive forcing calculated in the other simulations. The importance of reducing this disagreement is highlighted by this paper, which demonstrates that the warming due to soot influence on mixed-phase clouds has an upper bound comparable in magnitude to the best estimates of the cooling associated with anthropogenic aerosol effects on liquid clouds [*Forster et al.*, 2007], but also that even the sign of the radiative forcing associated with BC interactions with mixed-phase clouds is uncertain.

[26] An interesting extension of the study presented here would be to investigate various ice multiplication processes and their importance for aerosol effects on mixed-phase clouds. Furthermore, a treatment of aerosol effects on cirrus

clouds, accounting for heterogeneous and homogeneous freezing at temperatures below −38°C is currently being implemented in CAM-Oslo, allowing for simulations of aerosol effects on clouds at all cloud temperatures. Finally, a better quantification of the IN ability of BC, as well as changes in mineral dust loading in response to desertification and deforestation, will help to determine whether significant changes in IN concentrations since preindustrial times have in fact occurred. Recent publications (e.g., *Mahowald et al.* [2010]) indicate that dust loadings have undergone significant changes in the 20th century. In the future, we hope to explore how feedbacks associated with climate change influence dust emissions, as well as how these dust emissions in turn influence climate via their impact on mixed-phase clouds.

[27] **Acknowledgments.** This work was supported in part by the facilities and staff of the Yale University Faculty of Arts and Sciences High Performance Computing Center. We would like to acknowledge Jon Egill Kristjansson, Trond Iversen, Øyvind Seland, and Alf Kirkevåg for their important roles in the CAM-Oslo development, and we would like to thank three anonymous reviewers for comments that significantly improved the manuscript.

References

Abdul-Razzak, H., and S. J. Ghan (2000), A parameterization of aerosol activation: 2. Multiple aerosol type, *J. Geophys. Res.*, *105*, 6837–6844, doi:10.1029/1999JD901161.

Albrecht, B. (1989), Aerosols, cloud microphysics, and fractional cloudiness, *Science*, *245*, 1227–1230.

Austin, R. T., A. J. Heymsfield, and G. L. Stephens (2009), Retrieval of ice cloud microphysical parameters using the CloudSat millimeter-wave radar and temperature, *J. Geophys. Res.*, *114*, D00A23, doi:10.1029/2008JD010049.

Bond, T. C., B. Wehner, A. Plewka, A. Wiedensohler, J. Heintzenberg, and R. J. Charlson (2006), Climate-relevant properties of primary particulate emissions from oil and natural gas combustion, *Atmos. Environ.*, *40*, 3574–3587.

Collins, W. D., et al. (2006), The formulation and atmospheric simulation of the Community Atmosphere Model version 3 (CAM3), *J. Clim.*, *19*, 2144–2162.

Cozic, J., S. Mertes, B. Verheggen, D. Cziczo, S. J. Gallavardin, S. Walter, U. Baltensperger, and E. Weingartner (2008), Black carbon enrichment in atmospheric ice particle residuals observed in lower tropospheric mixed phase clouds, *J. Geophys. Res.*, *113*, D15209, doi:10.1029/2007JD009266.

DeMott, P. J. (1990), An exploratory study of ice nucleation by soot aerosols, *J. Appl. Meteorol.*, *29*, 1072–1079.

DeMott, P. J., A. J. Prenni, Z. Liu, S. M. Kreidenweis, M. D. Petters, C. H. Twohey, M. S. Richardson, T. Eidhammer, and D. C. Rogers (2010), Predicting global atmospheric ice nuclei distributions and their impact on climate, *Proc. Natl. Acad. Sci. U. S. A.*, *107*, 11,217–11,222.

Denman, K. L., et al. (2007), Couplings between changes in the climate system and biogeochemistry, in *Climate Change 2007: The Physical Science Basis. Contribution of Working Group I to the Fourth Assessment Report of the Intergovernmental Panel on Climate Change*, pp. 499–587, Cambridge Univ. Press, Cambridge, U. K.

Dentener, F., et al. (2006), Emissions of primary aerosols and precursor gases in the years 2000 and 1750 prescribed data-sets for AeroCom, *Atmos. Chem. Phys.*, *6*, 4321–4344.

Diehl, K., and S. K. Mitra (1998), A laboratory study of the effects of a kerosene-burner exhaust on ice nucleation and the evaporation rate of ice crystals, *Atmos. Res.*, *32*, 3145–3151.

Diehl, K., M. Simmel, and S. Wurzler (2006), Numerical simulations on the impact of aerosol properties and freezing modes on the glaciation, microphysics and dynamics of convective clouds, *J. Geophys. Res.*, *111*, D07202, doi:10.1029/2005JD005884.

Ebert, E. E., and J. A. Curry (1992), A parameterization of ice cloud optical properties for climate models, *J. Geophys. Res.*, *97*, 3831–3836, doi:10.1029/91JD02472.

Eidhammer, T., et al. (2010), Ice initiation by aerosol particles: Measured and predicted ice nuclei concentrations versus measured ice crystal concentrations in an orographic wave cloud, *J. Atmos. Sci.*, *67*, 2417–2436.

Eliasson, S., S. A. Buehler, M. Milz, P. Eriksson, and V. O. John (2010), Assessing modelled spatial distributions of ice water path using satellite data, *Atmos. Chem. Phys. Disc.*, *10*, 12,185–12,224.

Eriksson, P., B. Rydberg, M. Johnston, D. P. Murtagh, H. Struthers, S. Ferrachat, and U. Lohmann (2010), Diurnal variations of humidity and ice water content in the tropical upper troposphere, *Atmos. Chem. Phys. Disc.*, *10*, 11,711–11,750.

Fornea, A. P., S. D. Brooks, J. B. Dooley, and A. Saha (2009), Heterogeneous freezing of ice on atmospheric aerosols containing ash, soot, and soil, *J. Geophys. Res.*, *114*, D13201, doi:10.1029/2009JD011958.

Forster, P., et al. (2007), Changes in atmospheric constituents and in radiative forcing, in *Climate Change 2007: The Physical Science Basis. Contribution of Working Group I to the Fourth Assessment Report of the Intergovernmental Panel on Climate Change*, pp. 129–234, Cambridge Univ. Press, Cambridge, U. K.

Gettelman, A., X. Liu, S. J. Ghan, H. Morrison, and A. J. Conley (2010), Global simulations of ice nucleation and ice supersaturation with an improved cloud scheme in the Community Atmosphere Model, *J. Geophys. Res.*, *115*, D18216, doi:10.1029/2009JD013797.

Girard, E., J. P. Blanchet, and Y. Dubois (2004), Effects of arctic sulphuric acid aerosols on wintertime low-level atmospheric ice crystals, humidity and temperature at Alert, Nunavut, *Atmos. Res.*, *73*, 131–148.

Hallett, J., and S. C. Mossop (1974), Production of secondary ice particles during the riming process, *Nature*, *249*, 26–28.

Hoose, C., U. Lohmann, R. Erdin, and I. Tegen (2008), The global influence of dust mineralogical composition on heterogeneous ice nucleation in mixed-phase clouds, *Environ. Res. Lett.*, *3*, 025003, doi:10.1088/1748-9326/3/2/025003.

Hoose, C., J. E. Kristjánsson, T. Iversen, A. Kirkevåg, Ø. Seland, and A. Gettelman (2009), Constraining cloud droplet number concentration in GCMs suppresses the aerosol indirect effect, *Geophys. Res. Lett.*, *36*, L12807, doi:10.1029/2009GL038568.

Hoose, C., J. E. Kristjánsson, J.-P. Chen, and A. Hazra (2010), A classical-theory-based parameterization of heterogeneous ice nucleation by mineral dust, soot, and biological particles in a global climate model, *J. Atmos. Sci.*, *67*, 2483–2503, doi:10.1175/2010JAS3425.

Jiang, J. H., H. Su, S. T. Massie, P. R. Colarco, M. R. Schoeberl, and S. Platnick (2009), Aerosol-CO relationship and aerosol effect on ice cloud particle size: Analyses from Aura Microwave Limb Sounder and Aqua Moderate Resolution Imaging Spectroradiometer observations, *J. Geophys. Res.*, *114*, D20207, doi:10.1029/2009JD012421.

Kärcher, B., O. Möehler, P. J. DeMott, S. Pechtl, and F. Yu (2007), Insights into the role of soot aerosols in cirrus cloud formation, *Atmos. Chem. Phys.*, *7*, 4203–4227.

Korolev, A. (2007), Limitations of the Wegener-Bergeron-Findeisen mechanism in the evolution of mixed-phase clouds, *J. Atmos. Sci.*, *64*, 3372–3375.

Korolev, A., and G. A. Isaac (2006), Relative humidity in liquid, mixed phase and ice clouds, *J. Atmos. Sci.*, *63*, 2865–2880.

Korolev, A., and I. P. Mazin (2003), Supersaturation of water vapor in clouds, *J. Atmos. Sci.*, *60*, 2957–2974.

Kristjánsson, J. E., J. M. Edwards, and D. L. Mitchell (2000), Impact of a new scheme for optical properties of ice crystals on climates of two GCMs, *J. Geophys. Res.*, *105*, 10,063–10,079, doi:10.1029/2000JD900015.

Levin, Z., and W. Cotton (2007), Aerosol pollution impact on precipitation: A scientific review, report from the WMO/IUGG International Aerosol Precipitation Science Assessment Group (IAPSAG), World Meteorol. Organ., Geneva, Switzerland.

Levkov, L. B., B. Rockel, H. Kapitza, and E. Raschke (1992), 3D mesoscale numerical studies of cirrus and stratus clouds by their time and space evolution, *Contrib. Atmos. Phys.*, *59*, 35–58.

Liu, X., J. E. Penner, S. J. Ghan, and M. Wang (2007), Inclusion of ice microphysics in the NCAR Community Atmosphere Model version 3 (CAM3), *J. Clim.*, *20*, 4526–4547.

Lohmann, U. (2002), Possible aerosol effects on ice clouds via contact nucleation, *J. Atmos. Sci.*, *59*, 647–656.

Lohmann, U., and K. Diehl (2006), Sensitivity studies of the importance of dust ice nuclei for the indirect aerosol effect on stratiform mixed-phase clouds, *J. Atmos. Sci.*, *63*, 968–982.

Lohmann, U., and H. Feichter (2005), Global indirect aerosol effects: A review, *Atmos. Chem. Phys.*, *5*, 715–737.

Mahowald, N. M., et al. (2010), Observed 20th century desert dust variability: Impact on climate and biogeochemistry, *Atmos. Chem. Phys. Disc.*, *10*, 12,585–12,628.

McFarquhar, G. M., and A. J. Heymsfield (2002), Microphysical characteristics of three anvils sampled during the Central Equatorial Pacific Experiment (CEPEX), *J. Atmos. Sci.*, *53*, 2401–2423.

Möhler, O., et al. (2005), Effect of sulfuric acid coating on heterogeneous ice nucleation by soot particles, *J. Geophys. Res.*, *110*, D11210, doi:10.1029/2004JD005169.

Morrison, H., and A. Gettelman (2008), A new two-moment bulk stratiform cloud microphysics scheme in the Community Atmosphere Model, version 3 (CAM3). Part I: Description and numerical tests, *J. Clim.*, *21*, 3642–3659.

Pruppacher, H. R., and J. D. Klett (1997), *Microphysics of Clouds and Precipitation*, 2nd ed., Kluwer Acad., Norwell, Mass.

Rasch, P. J., and J. E. Kristjánsson (1998), A comparison of the CCM3 model climate using diagnosed and predicted condensate parameterizations, *J. Clim.*, *11*, 1587–1614.

Rossow, W. B., and R. A. Schiffer (1999), Advances in understanding clouds from ISCCP, *Bull. Am. Meteorol. Soc.*, *80*, 2261–2287.

Ryan, B. F. (1996), On the global variation of precipitating layer clouds, *Bull. Am. Meteorol. Soc.*, *77*, 53–70.

Salzmann, M., Y. Ming, J.-C. Golaz, P. A. Ginoux, H. Morrison, A. Gettelman, M. Kramer, and L. J. Donner (2010), Two-moment bulk stratiform cloud microphysics in the GFDL AM3 GCM: Description, evaluation, and sensitivity tests, *Atmos. Chem. Phys. Disc.*, *10*, 6375–6446.

Seland, Ø., T. Iversen, A. Kirkevåg, and T. Storelvmo (2008), Aerosol-climate interactions in the CAM-Oslo atmospheric GCM and investigation of associated basic shortcomings, *Tellus, Ser. A*, *60*, 459–491.

Stephens, G. L., et al. (2002), The CloudSat mission and the A-train: A new dimension of space-based observations of clouds and precipitation, *Bull. Am. Meteorol. Soc.*, *83*, 1771–1790.

Stevens, B., and G. Feingold (2009), Untangling aerosol effects on clouds and precipitation in a buffered system, *Nature*, *461*, 607–613.

Storelvmo, T., J. E. Kristjánsson, S. J. Ghan, A. Kirkevåg, Ø. Seland, and T. Iversen (2006), Predicting cloud droplet number concentration in Community Atmosphere Model (CAM)-Oslo, *J. Geophys. Res.*, *111*, D24208, doi:10.1029/2005JD006300.

Storelvmo, T., J. E. Kristjánsson, and U. Lohmann (2008a), Aerosol influence on mixed-phase clouds in CAM-Oslo, *J. Atmos. Sci.*, *65*, 3214–3230.

Storelvmo, T., J. E. Kristjánsson, U. Lohmann, A. Kirkevåg, Ø. Seland, and T. Iversen (2008b), Modeling of the Wegener-Bergeron-Findeisen process: Implications for aerosol indirect effects, *Environ. Res. Lett.*, *5*, 019801, doi:10.1088/1748-9326/3/4/055001.

Storelvmo, T., J. E. Kristjánsson, U. Lohmann, A. Kirkevåg, Ø. Seland, and T. Iversen (2010), Corrections to modeling of the Wegener-Bergeron-Findeisen process: Implications for aerosol indirect effects, *Environ. Res. Lett.*, *5*, 019801, doi:10.1088/1748-9326/5/1/0198013.

Targino, A. C., et al. (2009), Influence of particle chemical composition on the phase of cold clouds at a high-alpine site in Switzerland, *J. Geophys. Res.*, *114*, D18206, doi:10.1029/2008JD011365.

Twomey, S. (1977), The influence of pollution on shortwave albedo of clouds, *J. Atmos. Sci.*, *34*, 1149–1152.

Waliser, D. E., et al. (2009), Cloud ice: A climate model challenge with signs and expectations of progress, *J. Geophys. Res.*, *114*, D00A21, doi:10.1029/2008JD010015.

Wood, R. (2006), Cancellation of aerosol indirect effects in marine stratocumulus through cloud thinning, *J. Atmos. Sci.*, *64*, 2657–2669.

Wyser, K. (1998), The effective radius in ice clouds, *J. Clim.*, *11*, 1793–1802.

Zeng, X. P., W. K. Tao, M. H. Zhang, A. Y. Hou, S. Xie, S. Lang, X. W. Li, D. O. Starr, and X. F. Li (2009), A contribution by ice nuclei to global warming, *Q. J. R. Meteorol. Soc.*, *135*, 1614–1629.

P. Eriksson, Department of Earth and Space Science, Chalmers University of Technology, SE-41296 Gothenburg, Sweden.

C. Hoose, Institute for Meteorology and Climate Research, Karlsruhe Institute of Technology, Hermann-von-Helmholtz-Platz 1, D-76344 Karlsruhe, Germany.

T. Storelvmo, Department of Geology and Geophysics, Yale University, 210 Whitney Ave., New Haven, CT 06511, USA. (trude.storelvmo@yale.edu)